Supplement Materials for

Construction of ^{124}I-trastuzumab for noninvasive HER2 detection: From patient-derived xenograft models to gastric cancer PET imaging

Xiaoyi Guo[1, †], Nina Zhou[1, †], Zuhua Chen[2, †], Teli Liu[1], Xiaoxia Xu[1], Xia Lei[1], Lin Shen[2], Jing Gao[2], Zhi Yang[1, ✉] Hua Zhu[1, ✉]

† These authors contributed equally to this work

[1.] Key Laboratory of Carcinogenesis and Translational Research (Ministry of Education/Beijing), Department of Nuclear Medicine; Peking University Cancer Hospital & Institute, Beijing, 100142, China

[2.] Department of Gastrointestinal oncology, Peking University Cancer Hospital & Institute, Beijing 100142, China

Article submitted to: Gastric Cancer

Version: 1

* For correspondence or reprints contact either of the following:

Corresponding author:

Zhi Yang, PhD, Beijing Cancer Hospital, Department of Nuclear Medicine, No. 52 Fucheng Rd., 100142, Beijing, China.

Tel.: +86-10-88196196, Fax: +86-10-88196196, E-mail: pekyz@163.com

Hua Zhu, PhD, Beijing Cancer Hospital, Department of Nuclear Medicine, No. 52 Fucheng Rd., 100142, Beijing, China.

Tel.: +86-10-88196196, Fax: +86-10-88196196, E-mail: zhuhuananjing@163.com

Radiolabel, Quality Control and Stability

Trastuzumab was labeled by the N-bromosuccinimide (NBS) method with ^{124}I. Briefly, formulations of 37 MBq ^{124}I/200 μg trastuzumab were produced under current Good Manufacturing Practice (cGMP) conditions. Briefly, trastuzumab was incubated with ^{124}I and 12 μg NBS in 0.1 M pH 7.4 phosphate buffer. After a 1-minute incubation, the mixture was purified by a PD-10 column and subject to terminal sterilization through a 0.22-μm filter. The production of ^{124}I-trastuzumab proved to be sterile and endotoxin free.

The radiochemical purity and stability of ^{124}I-trastuzumab were confirmed by radioactive thin-layer chromatography (radio-TLC) (Bioscan, IAR-2000, Washington, DC, USA) and high-performance liquid chromatography (HPLC) (Agilent, Lake Forest, CA, USA). Radio-TLC was performed with silica-impregnated glass fiber sheets (TLC-SG) (Agilent, USA) cut to 2.0x10 cm in size, and 0.01 M EDTA in saline was used for elution. The HPLC system was equipped with both a UV absorption detector and a B-Fc-1000 HPLC radioactivity detector (Bioscan, Washington, DC, USA). The radioactivity was determined with an instant chromatography scanner (Merker Gmbh, Germany) equipped with an ionization chamber. A solution of 0.01 M pH 7.4 sodium phosphate buffer (PBS) was used as a mobile phase. The ^{124}I radiolabeling was performed under good-laboratory-practice conditions with quality control, as shown in **Table S1**. The formulation of ^{124}I-trastuzumab proved to be sterile and endotoxin-free. As shown in **Figure S1**, the radio-TLC of ^{124}I showed good quality, and the radiochemical purity after purification reached 99.2%. The radio-HPLC analysis of the radiopharmaceuticals revealed no aggregates, fragments, or radioactive impurities.

Table S1. Production and quality control of ^{124}I-trastuzumab

Parameter	QC Specification	QC Result
Appearance	Clear, colourless	Pass
Volume	1.0-2.0 mL	1.5 mL
pH	5.0-8.0	7.4
Radio-TLC	> 95%	> 99%
Radio-HPLC	> 95%	> 99%
Ethanol	< 5%	0
Endotoxins	< 15 EU/mL	<0.05 EU/ml
Sterility	Sterile	Pass
Specific Activity	13.5-100 GBq/μmol	25 GBq/μmol

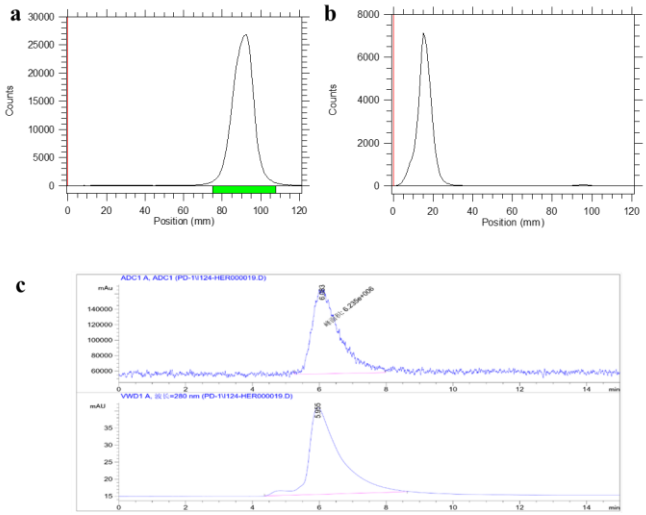

Figure S1. **a** The radio-TLC chromatograph of ^{124}I-trastuzumab; **b** The radio-TLC chromatograph of ^{124}I-trastuzumab; **c** The radio-HPLC chromatograph of ^{124}I-trastuzumab.

^{124}I-trastuzumab appeared to be rather stable, with mean decreases in radiochemical purity of less than 5.0% in both saline at 4 ℃ and 5% HSA at 37 ℃ after a 96 h incubation.

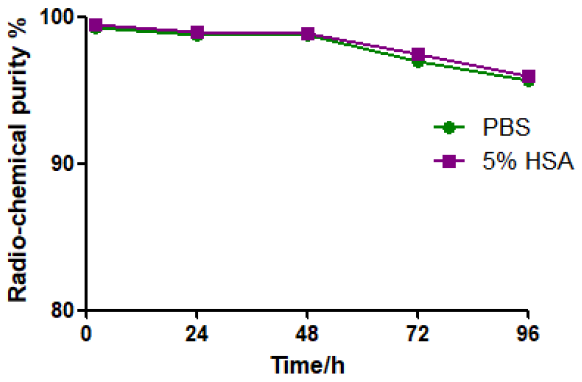

Figure S2. The stability of ^{124}I-trastuzumab in 5% HSA and saline.

Micro-PET Imaging of ^{64}Cu-NOTA-trastuzumab and ^{124}I-trastuzumab

HER2-positive (n = 20) and HER2-negative (n = 20) patient-derived xenografts (PDX) were constructed based on the methods we previously described. When the tumor volume reached 0.5-1.0 cm in diameter, the mice were randomly assigned into groups. A thyroid iodine uptake blockade by an oral administration of 5 ‰ potassium iodide was initiated 3 days before and throughout the full study process. For micro-PET imaging, all mice were subjected to isoflurane anesthesia (1-2%) with air and were then placed on a tube with self-adjusting temperature capabilities to maintain a constant body temperature throughout the procedure. The mice were visually monitored for breathing and other signs of distress throughout the full imaging period. The images were reconstructed using a

three-dimensional ordered-subsets expectation maximum algorithm (OSEM) without attenuation correction.

Comparing the whole-body distribution of ^{64}Cu-NOTA-trastuzumab and ^{124}I-trastuzumab, there appeared to be a statistically significant differences in the radioactivity uptake in the liver and background tissues, as shown in **Figure S3**.

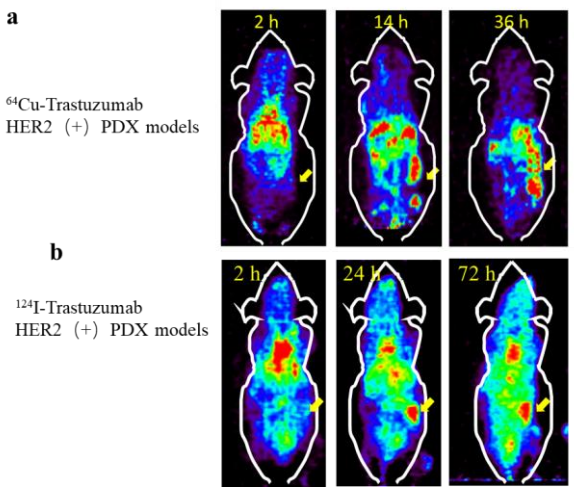

Figure S3. **a** Whole-body coronal microPET images of ^{64}Cu-NOTA-trastuzumab and ^{124}I-trastuzumab in HER2-positive PDX models at 2, 14, and 36 h. **b** Whole-body coronal microPET images of ^{124}I-trastuzumab in HER2-positive PDX models at 2, 24, and 72 h.

The tumor uptake was not significantly different between ^{124}I-trastuzumab and ^{64}Cu-NOTA-trastuzumab. ^{124}I-tratuzumab achieved higher imaging contrast than ^{64}Cu-NOTA-trastuzumab because of less nonspecific uptake and better tumor-to-soft-tissue ratios. The ^{124}I-trastuzumab T/L ratio was 1.93±0.017 at 24 h compared with the ^{64}Cu-NOTA-trastuzumab T/L ratio of 0.95±0.029 at 14 h (p< 0.0001, n=3), and the ^{124}I-trastuzumab T/L ratio was 2.26±0.069 at 72 h compared with the ^{64}Cu-NOTA-trastuzumab T/L ratio of 1.14±0.094 at 36 h (p< 0.0001, n=3). In addition, the ^{124}I-trastuzumab T/M ratio was 9.87±0.095 at 24 h compared with the ^{64}Cu-NOTA-trastuzumab T/M ratio of 10.59±0.025 at 14 h (P=0.003, n=3), and the ^{124}I-trastuzumab T/M ratio was 17.27±0.76 at 72 h compared with the ^{64}Cu-NOTA-trastuzumab T/M ratio of 7.13±0.49 at 36 h (p< 0.0001, n=3). A high T/L ratio is helpful for detecting small liver metastases. A higher T/M ratio allows for clear lesion visualization.

Autoradiography

The autoradiography analyses demonstrated that the tumor uptake of ^{124}I-trastuzumab in the HER2-positive PDX models was higher than that of ^{124}I-hIgG1 in the HER2-positive PDX models and higher than that of ^{124}I-trastuzumab in the HER2-negative PDX models, as shown in **Figure S4**.

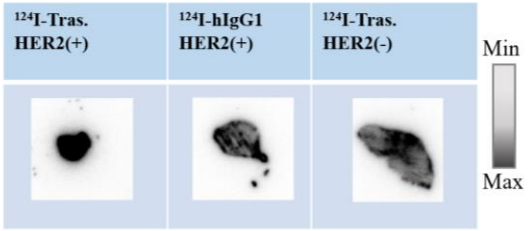

Figure S4. Full view of the autoradiography analysis of ^{124}I-trastuzumab in ^{124}I-Tras. (HER2+), ^{124}I-hIgG1. (HER2+) and ^{124}I-Tras. (HER2-). The yellow arrow indicates the tumor.

Patient Enrollment

All patients provided written informed consent before participating in the study. The patients included in this study had pathologically confirmed HER2-positive (IHC 3+ or 2+ and FISH+) or HER2-negative (IHC 2+/FISH-) advanced GC/EGC and were aged between 20 and 75 years. The main exclusion criteria were if the patient had congestive heart failure, had severe liver or kidney dysfunction, was pregnant or lactating, had known hypersensitivity to trastuzumab or could not lie in the scan bed for more than 1 h. A HER2-positive biopsy was allowed to be from any time during the patient's disease course and could be from the primary cancer or a metastatic lesion. A cohort of 6 patients (GC n=3, and EGC n=3) with pathologically confirmed AGC/EGC treated in our department at Peking University Cancer Hospital from June 2018 to December 2018 were included.

^{124}I-trastuzumab and ^{18}F-FDG PET/CT Imaging in GC/EGC Patients

All images were acquired with a PET/CT scanner (Biograph64, Siemens, Erlangen, Germany). The acquisition was carried out in Flow Motion 3-dimensional mode (bed entry speed, 1 mm/s) from the apex of the skull to the mid-thigh, and the PET axial field of view was 21.6 cm. The PET images were reconstructed by the TrueX+TOF method. Low-dose CT scans were acquired in CARE Dose4D mode (120 kV, image slice thickness, 3.0 mm). A Siemens workstation (MultiModality Workplace) was used for postprocessing. The PET/CT images were interpreted by two experienced nuclear radiologists, and the results were checked by two independent physicians.

Biodistribution of ^{124}I-trastuzumab in patient 2

The whole-body distribution of ^{124}I-trastuzumab in patient 2 is shown in Figure S5. The regional time–activity curves of ^{124}I-trastuzumab in the main organs of patient 2 at 1, 24, 48, 72, and 120 h are shown in Figure S6.. At 1 h, ^{124}I-trastuzumab mainly existed in the circulatory system and in the well-perfused organs (including liver, spleen, and kidney). The SUVmax in the blood showed a high value of 9.8 at 1 h and decreased at 24, 48, 72, and 120 h. The uptake in the liver and spleen decreased at 24, 48, 72, and 120 h. The uptake in the kidneys slightly increased at 24 h and decreased at 48, 72,

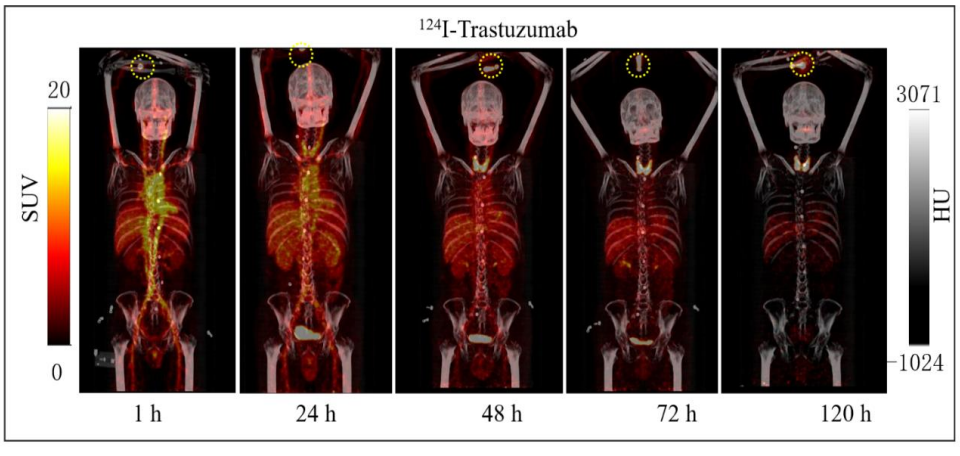

and 120 h. In contrast, the uptake in the urinary bladder was visualized at 1 h, showed a rapid increase at approximately 24 h, and decreased at 72 and 120 h. Uptake in the thyroid was low at 1 h and 24 h but increased at 48, 72, and 120 h.

Figure S5. Whole-body PET images (MIP) of ^{124}I-trastuzumab in patient 2 at 1, 24, 48, 72, and 120 h post-injection. The yellow dotted circle is a 1% reference internal standard.

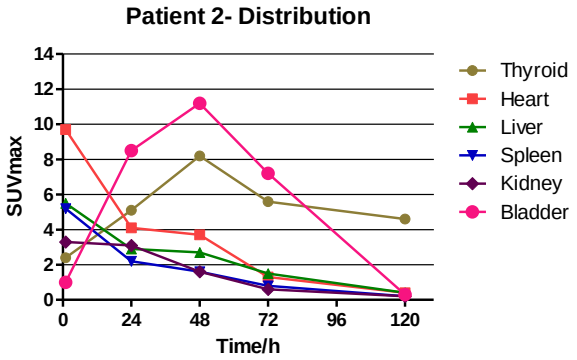

Figure S6. The regional time-activity curves of ^{124}I-trastuzumab in patient 2.

Radiation Dosimetry

Organ activity concentration data were obtained by drawing regions of interest (ROIs) on the PET images for the following organs/tissues: liver, kidneys, blood (left ventricular chamber), spleen, muscle, subcutaneous fat and red marrow. The red marrow activity concentrations were determined from the average activity concentration measured in the lumbar vertebrae. Image-derived SUVLBM was converted to activity concentration per unit of mass (KBq/g), and areas under the curve (AUCs) were estimated by trapezoidal integration. Whole-organ AUCs were estimated by multiplying the activity concentration from the AUCs by the projected organ mass. The residence times were derived by dividing the whole-organ AUCs by the administered activity. The residence time for the remainder of the body was derived by subtracting all individually estimated residence times from the whole-body residence time. Thereafter, the absorbed radiation doses to the individual organs were calculated using the OLINDA/EXM software application.

Pathological examination

Figure S7 shows the HE staining, IHC and FISH of patient 3, who was a HER2-positive patient confirmed to have a high level (HER2 3+/FISH-) of HER2/neu expression, and patient 6 was a HER2-negative patient confirmed to have a low level (FISH-) of HER2/neu expression.

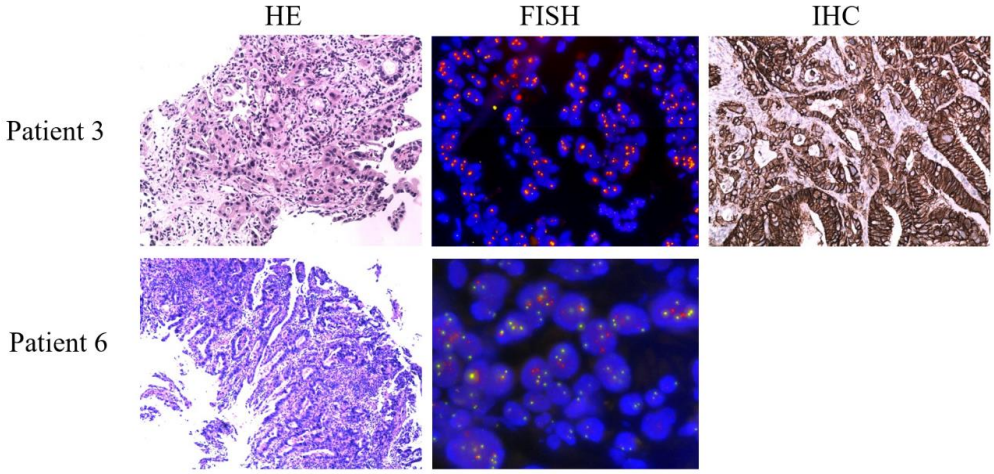

Figure S7. HE staining, IHC and FISH of HER2-positive patient 3 and HER2-negative patient 6.